Sedapp v2021: a non-linear diffusion-based forward stratigraphic model for shallow marine environments

Jingzhe Li[1, 2], Piyang Liu[3], Shuyu Sun[4] (✉), Zhifeng Sun [2, 1], Yongzhang Zhou[5], Liang Gong[6], Jinliang Zhang[7], Dongxing Du[1,2]

1. College of Electromechanics, Qingdao University of Science and Technology, Qingdao 266061, China
2. Geo-Energy Research Institute, Qingdao University of Science and Technology, Qingdao 266061, China
3. School of Science, Qingdao University of Technology, Qingdao, 266520, China
4. King Abdullah University of Science and Technology, Jeddah 23955-6900, Saudi Arabia
5. School of Earth Science and Geological Engineering, Sun Yat-sen University, Guangzhou 510275, China
6. School of New Energies, China University of Petroleum (EastChina), Qingdao 266555, China
7. Department of Geography, Beijing Normal University, Beijing 100875, China

Correspondence to: Shuyu Sun (frank.sun.sa@gmail.com)

Abstract

The formation of stratigraphy in shallow marine environments has long been an important topic within the geologic community. Although many advances have been made in the field of forward stratigraphic modelling (FSM), there are still some areas that can be improved in the existing models. In this work, the authors present our recent development and application of Sedapp: a new non-linear open-source R code for FSM. This code uses an integrated depth-distance related function as the expression of the transport coefficient to underpin the FSM with more along-shore details. In addition to conventional parameters, a negative-feedback sediment supply rate and a differentiated deposition-erosion ratio were also introduced. All parameters were implemented in a non-linear manner. Sedapp is a 2DH tool that is also capable of running 1DH scenarios. Two simplified case studies were conducted. The results showed that Sedapp can not only assist in geologic interpretation, but is also an efficient tool for internal architecture predictions.

Keywords: Forward stratigraphic modelling, continental shelf, R codes, fluvial-deltaic, continental fault basin

1 Introduction

Shallow marine areas are among the most active environments for sedimentation, where sea level, tectonism, climate all influence the interactions between land and sea. The sedimentary successions formed in these areas are an important record of the past interactions. In addition, shallow marine stratigraphic record itself can be an ideal hydrocarbon accumulation place. From this record, many theoretical and field studies have made great achievements and accumulated a wealth of data in the past decades.

In order to better interpret the specific processes and analyze internal architectures, many forward stratigraphic models (FSM) have been built for a range of temporal and spatial scales. These models can be roughly divided into two categories, according to their purposes. The first is a full source-to-sink type, which mainly analyzes the deposition and erosion processes from the perspective of the whole sediment chain. In addition to analyzing the depositional response in the downstream unloading area, this kind of model also deals with precipitation and tectonic uplift in the upstream catchments area, which directly determine water and sediment flux (Armitage et al., 2011;2018; Ding et al., 2019; Guerit et al., 2019; Zhang J.Y. et al., 2020). The second, which we choose here, is a sink-dominant type, which focuses on analyzing the architectures and stacking patterns of the sedimentary results in a forward manner (Rivenaes, 1997; Dalman and Weltje, 2012; Granjeon, 2014; Li et al., 2020). This type generally does not consider how the sediments in the source area are entrained. Instead, it usually takes the sediment supply rate as a known condition. This kind of model is appropriate for rapid evaluation of the underground strata and prediction of potential hydrocarbon reservoirs by fitting some known evidences.

For long-term processes, sediment flux is usually assumed to be proportional to the topographic gradient. Thus, through the mass conservation law, a diffusion equation like Eq. (1) is generally used in FSM models (Paola, 2000).

$$\frac{\partial h}{\partial t} = \nabla \cdot \left(\Gamma \nabla h \right)$$

(1)

where h denotes the topography, t denotes the time and Γ denotes the transport coefficient. If Γ is a constant or it does not change with the unknowns, these models are usually called linear models. Whereas if Γ changes with the primary unknown h, these models are called non-linear models.

In many cases, linear models are not very robust when the stratigraphic results and controlling factors are interactively connected. For example, topography evolution in the marine portion is seriously affected by the water depth, whereas water depth is generally a function of topography and sea level. In this case, non-linear models seem to be more suitable. Many existing non-linear models define the transport coefficient using water depth-related functions (e.g., in Clarke et al .1983; Kaufman,1991; Syvitski and Hutton, 2001, the coefficient value was assumed to decrease exponentially with the water depth). Water depth models can work well in general coastal zones. However, in shallow marine environments with river injection, these models are not as effective, especially when reflecting the shoreline shape in plane view. Depositional processes around the river mouth are more active than those at a distance, even when they are at the same water depth.

Additionally, according to Eq. (1), if Γ is fixed for a given site, deposition or erosion (i.e., $\partial h/t > 0$ or $\partial h/\partial t < 0$) depend solely on the topographic gradient. However, in a basin, the efficiency of deposition and erosion can be very different, even if the slope, sediment supply, and water flux are the same. For example, some bed surface is "hardground", which is very difficult to erode. While the overlying deposition process is relatively easy. In this case, a distinction between the two processes seems necessary. For a long-term stratigraphic forming process, there may exist many sedimentary discontinuities, which may provide long enough time to generate a variety of "hardgrounds" (the missing time in the sedimentary record can be predominant according to Miall, 2015). This is actually related to the efficiency ratio of deposition to erosion. While customizable adjustment of this ratio is less involved in the existing FSM models. Although some source-to-sink models (e.g. Guerit et al., 2019) have introduced the distinction between deposition and erosion processes, the complex parameter settings still severely limit its practicability in a quick result-fitting. In addition, many existing models are not free or open-source, making it difficult for people to reproduce and improve them.

In this paper, we propose a new non-linear FSM model, which is expected to add some new features to the existing models. This model is integrated into a framework called Sedapp, which is an open-source and cross-platform application written in R. We use examples to show how this model

works and test its effectiveness and convenience in reconstruction of sedimentary systems, revealing their internal architectures.

2 Methodology

2.1 Mathematical model

The Sedapp mathematical model can be expressed as follows:

$$F_i \frac{\partial h}{\partial t} = \max\left(\nabla \cdot (\Gamma_i \nabla h), \frac{1}{Der} \nabla \cdot (\Gamma_i \nabla h) \right) + q \tag{2}$$

$$\sum_i^n F_i = 1 \tag{3}$$

where F_i is the fraction of the ith class of sediment, h is elevation, t is time, ∇ is the nabla operator, Der is a user-defined parameter denoting the ratio of deposition to erosion (it can be a scalar, vector or tensor value depending on its temporal and spatial variability), Γ_i is the diffusion coefficient for the ith class of lithology, and q is the source term that is a function of coordinates and time (the source term is used only for endogenetic sedimentation, especially carbonates. If endogenetic sedimentation is ignored, the source term can be left out). Of these, h and F_i are the primary unknowns.

Note that Γ_i cannot be outside the parentheses because they are not constants but rather functions of spatial coordinates and time. The Γ can generally be expressed as:

$$\Gamma = \max(\alpha\, e^{-\frac{D(\mathbf{x},h,sl)^{\eta}}{\beta}}, \ \alpha_{wd} e^{-\frac{Wd(\mathbf{x},h,sl)^{\eta_{wd}}}{\beta_{wd}}}) + \varepsilon \tag{4}$$

where α/α_{wd} are preexponential factors (L^2/T) , η/η_{wd} are distance indexes (no dimension), β/β_{wd} are spatial scale factors (L^{η} or $L^{\eta_{wd}}$), and ε is an adjustment factor (L^2/T) reflecting the environment energy. In particular, the distance function $D=D(\mathbf{x},h,sl)$ and water depth function $Wd(\mathbf{x},h,sl)$ change with spatial coordinates $\mathbf{x}$, topography h and the sea level sl, and they apply to the marine portion only.

When $Der = 1$ and n = 2, the 3D (actually 2DH, because h is another dimension perpendicular to x and y) scenario for Eq. (2) and Eq. (3) can also be expressed as:

$$F \frac{\partial h}{\partial t} = \frac{\partial}{\partial x}\left(\Gamma_1 \frac{\partial h}{\partial x} \right) + \frac{\partial}{\partial y}\left(\Gamma_1 \frac{\partial h}{\partial y} \right) + q(x, y, t) \tag{5}$$

$$(1-F)\frac{\partial h}{\partial t} = \frac{\partial}{\partial x}\left(\Gamma_2\frac{\partial h}{\partial x}\right) + \frac{\partial}{\partial y}\left(\Gamma_2\frac{\partial h}{\partial y}\right) + q(x,y,t) \tag{6}$$

where x and y are spatial coordinates. This is especially suitable for cases dealing only with two classes of sediments for simplicity, where Γ_1 is the transport coefficient for sand and Γ_2 is the transport coefficient for mud.

For 2D (1DH) scenarios, especially along the section line through the river mouth, the distance related term is generally larger than the water depth related term, so the latter term within the max function in Eq. (4) is usually omitted. For convenience in coding, also ignoring the endogenetic sedimentation, Eq. (5), Eq. (6) and Eq. (4) can be simplified into:

$$F\frac{\partial h}{\partial t} = \frac{\partial}{\partial x}\left(\Gamma_1\frac{\partial h}{\partial x}\right) \tag{7}$$

$$(1-F)\frac{\partial h}{\partial t} = \frac{\partial}{\partial x}\left(\Gamma_2\frac{\partial h}{\partial x}\right) \tag{8}$$

$$\Gamma_i = \alpha_i \cdot e^{-\frac{(c\cdot D(\mathbf{x},t))^2}{E}} + \varepsilon, i = 1,2 \tag{9}$$

The joint effect of c and E in Eq. (9) is equivalent to that of β in Eq. (4). The variable c here, with a dimension of L^{-1}, is mainly used to facilitate the scale of distance and differentiate the transport characteristics of different sediment types (e.g., sand and mud). E is a dimensionless constant that represents hydraulic characteristic energy.

2.2 Code Implementation

Sedapp was written in the R language and its solution was based on the finite volume method (FVM), which has the desired property of local mass conservation and has a clear physical meaning (Versteeg and Malalasekera, 2007; Moukalled et al., 2016; Liu P. et al., 2017). The cell-centered variable arrangement method was used to store the unknowns at the grid element centroids. The non-linearity was implemented through stepwise iteration (Fig.1).

The brief work-flow within a single time step is as below:

1) Implement user-defined tectonic subsidence and update the topography;

2) Implement user-defined sea level and identify/update the shoreline location;

3) Solve the differential deposition/erosion function;

4) Implement the compaction and isostatic subsidence.

Step 3) is an important step. According to the hypothesis of diffusion-based FSM models, the change rate (by either deposition or erosion) is proportional to the gradient of the slope (Fernandes et al., 1997; Pelletier, 2013). If we use the diffusion equation/law directly without any differential treatments between deposition and erosion (in other words, Der is held at 1), it will be very difficult to treat some complex situations. For example, some bed surface is "hardground", which is very difficult to erode, whereas the overlying deposition process is relatively easy. Hence, for a given location, erosion and deposition could occur at different rates and Der may not be equal to 1. For example, if we wanted the erosion rate to be only 1/100 of the deposition rate, Der can be set to 100. Through the max() function in Eq. (2), for a deposition process (namely the $\frac{\partial h}{\partial t} > 0$), $\nabla \cdot (\Gamma_i \nabla h)$ would be larger than $\frac{1}{der} \nabla \cdot (\Gamma_i \nabla h)$, and $\nabla \cdot (\Gamma_i \nabla h)$ is used. Otherwise, the $\frac{1}{der} \nabla \cdot (\Gamma_i \nabla h)$ is used. If a non-erosion case is desired, Der can be set to a very large value.

Generally, sediment supply rate cannot be directly defined through boundary condition settings since the latter can only determine the boundary slope. Therefore, Sedapp uses a negative-feedback strategy to define the sediment supply rate. At each time step, the total amount of deposition within a step is first calculated using the previously defined α_{test}, and then the adjusted α_{mod} is calculated by Eq. (10):

$$\alpha_{mod} = \alpha_{test} \frac{V_{expected}}{V_{test}} \tag{10}$$

where α_{mod} denotes the modified α of this time step; $V_{expected}$ denotes the expected sediment increment, namely the sediment supply rate; and V_{test} denotes the computed sediment increment with α_{test}.

3 Characteristics

3.1 Nonlinear transport coefficients

The nonlinear transport coefficient is a feature of Sedapp. Sedapp's transport coefficient uses a function of both the distance from the estuary and the water depth. This feature makes it easier to simulate fluvial-deltaic processes in 2DH scenarios, which can reflect changes along the shore. Even in 1DH cases, this feature also has some advantages (see the discussion section for details).

Generally, a smaller c value in Eq. (9) results in a higher sediment travel distance and a larger

distribution range when the total amount of sediment is fixed. For example, the c of mud is usually set to 50%-85% of sand, thus reflecting the differential deposition of sand and mud. In addition, the environment energy ε can also influence the sediment travel distance; e.g. a larger ε will make the sediment travel further. As sedimentation progresses, the position of the estuary may change, so the distance from the estuary is updated at each time step to achieve the nonlinearity of Γ.

3.2 Differential and customizable deposition/erosion rate

During the actual deposition process, the properties of the underlying strata (such as compaction degree, lithology, and age, etc.), as well as some external environmental factors (such as temperature, humidity and pH value, etc.), will affect the erosion rate. Therefore, the customized treatment of erosion rate is another Sedapp characteristic.

In Sedapp, the deposition rate is a parameter that can be specified directly (for the adjustment process see section 2.2). Furthermore, the Der parameter is a user-defined parameter that controls the ratio of deposition rate to erosion rate. When Der is 1, the deposition rate is equal to the denudation rate (Fig.2a), and when Der value is 10 or 100, denudation is significantly weakened (Fig.2b). Theoretically, if the value of Der is large enough, it is equivalent to completely eliminating the denudation effect. Der values should be customized according to the actual situation.

3.3 Customizable compaction

Compaction is an important geological process after sediment deposition, especially when the sediment thickness is very high. In Sedapp, the compaction process can be easily realized by setting the composition of lithology and porosity curves.

In this paper, we designed a pyramid-shaped mountain simulation commonly used by other researchers (as shown in Fig.3, see Rivenaes, 1992 and Yuan et al., 2019 for reference). The Der value was set to 1. The sediment supply ratio of sand and mud was set to 1:1, and the porosity curve was set as shown in Fig.3d. After simulation, the top of the pyramid was denuded and the foot of the pyramid had deposited sediment of a given thickness.

To illustrate the effect of compaction, Sedapp introduces a scale factor that can enlarge the longitudinal scale. Fig.3a shows the original compression scale (that is, the scale factor was equal to 1), and the scale factors in Fig.3b and Fig.3c were 100 and 1000, respectively. It can be seen that sediment

thickness at the foot of the pyramid in Fig.3c was significantly smaller than that in Fig.3a. The factors that caused these differences were not only depth but also the proportion of sand and mudstone and the shape of depth-porosity curves, which can be easily adapted to different scenarios by modifying the lithologic proportion and porosity-depth functions in Sedapp.

4 Verification of Sedapp

To identify how well the algorithm works within geological context, some simple benchmark simulations are given below.

4.1 Typical stacking patterns

Typical stacking patterns including forced regression, normal regression, and transgression can be formed (Fig.4) by fixing sediment supply while controlling the adjusted sea level rise rate.

During the period of sea-level decline, the shoreline moved seaward, and the onlap points also moved seaward and form the offlap and downlap stratigraphic termination structures (Fig.4a). During slow sea-level rise, the shoreline continued to move seaward, but the onlap points started to move landward, forming an onlap termination structure. At the other end, the downlap structure continued to exist. During rapid sea-level rise, the shoreline started to move landward and the onlap points also moved landward. At this time, downlap structure did not exist above the slope break, but may have existed below the slope break.

4.2 Typical two-cycle scenario

To demonstrate the complete base level changing process, this paper designed a simulation with two full sinusoidal cycles as shown in Fig.5. In the first cycle, the shoreline dropped and moved seaward. Then it slowly rose and gradually moved landward until it reached the highest point and tended to stabilize. The water depth of deposition in the strata gradually deepened from left to right on the marine side (Fig.5a), and the sandy content reached a maximum around the shoreline (Fig.5b) near the shoreline. In the strata on the land side, the sand content was stratified. The sand content was relatively large during the early transgression and subsequently relatively small. The second cycle was located above the first cycle and continued the same characteristics as the first cycle, but the deposition range was enlarged and the average single layer thickness was thinner..

4.3 Case studies

1) Model 1

In order to better display the 2DH performance of Sedapp, this paper designed Model 1. Its length and width ranges were both 200m, and the elevation range was about 10m. The mesh was 200 × 200 in x-y plane. The time span of the model was set at 10 Myr, and the step size was set at 0.5 Myr. Sea level was kept constant at 3 m. The initial topography was set as shown in Fig.6a. A river was set up in the central position of the y-axis (y = 100m). The channel shape of the river was set in advance as a sine curve. The fluvial profile slope was set to a constant of 0.00357, and the sediment supply rate was not defined since it could vary according to the fluvial profile slope. The other main parameters of the model are shown in Tab. 1.

Projection of the simulation results on the x-y plane clearly showed the variability along the shore (Fig.7). When t = 0, the shoreline was a straight line, and the channel was in the middle of the shoreline. As time went on, the river mouth continued to move forward. From 0 to 2 Myr, the channel first swung to the north, then to the south, and the shoreline began to bulge slightly towards the sea side. From 2Myr, the channel continued to swing southward, until the time approached 4Myr and the river mouth began to slowly turn north. From 4Myr to 6Myr, the channel continued to swing northward, and the convex part towards the sea side became more prominent. From 6Myr to 8Myr, the channel continued the previous trend, while the convex shoreline became asymmetrical (increasing skewness to the north). From 8 Myr to 10 Myr, the principal line of the channel moved southward, and the convex shoreline gradually returned to being symmetrical (Fig.7).

The simulation results also revealed some interesting features in longitudinal sections (Fig.8). Two sections (y = 75m and y = 125m) perpendicular to the shoreline direction were selected (see Fig.7f for the position of the section line). The two sections are located on the north and south sides of the main channel. The distance between the channel and the two sections was variable. In the southern profile (y = 75m), from 4 Myr to 10 Myr, the isochronous lines of the formation changed from sparse to dense, and then from dense to sparse (i.e., the thickness of a single clinoform changed from thick to thin first and then from thin to thick) (Fig.8). This was completely contrary to what was observed in the northern profile (y = 125m). From 4Myr to 10Myr, the isochronous lines first changed from dense to sparse, and then from sparse to dense, reflecting that the deposition rate first increased and then

decreased (Fig.9).

Under the parameters shown in Tab. 1, due to the existence of estuaries, the shoreline bulged towards the sea side. A closer distance to the river mouth would result in a higher sedimentation rate and a greater shoreline advancing speed. From 2 Myr, the convex shape of the shoreline towards the sea side became more apparent, similar to the morphology of some real-world deltas (Fig.10).

2) Model 2

This code can be applied not only to marginal marine environments but also to the continental fault basins. Taking the 3 + 4 sand groups of the third member of Shahejie Formation in the Gaobei slope belt of Nanpu Sag in Bohai Bay Basin as an example, we conducted a simplified 1DH real case study. The basic geological background is as follows: During the deposition period of this set of strata, the normal fault tectonic movement in the north of the sag was active, which was the main controlling factor leading to the increase of accommodation space. At the same time, the terrigenous clasts came from the north is sufficient, and the basin was in a balanced state (Li et al., 2018). According to the geological background, a simplified reconstruction model (Model 2) was designed, which assumed that the subsidence rate of the boundary fault and sediment supply rate is constant, neglected the effect of isostasy, and considered the effect of sediment compaction.

The simulation results are shown in Fig.11. From the perspective of temporal and spatial stratigraphy, the shoreline mainly moved towards the sag center during the early stage, and then moved back to the land side. The deepest water depth occurred in the middle south part at 2 Myr (Fig.11a). This shoreline phenomenon is usually called autoretreat (Muto and Steel, 2002). The sand fraction section shows that the steep slope belt in the north was richer in sand content than the south (Fig.11b). The porosity section shows that porosity generally decreased from bottom to top. The porosity also varied horizontally, especially when the depth was greater than 800 m. The porosity in the north was higher than in the south.

Due to the over-simplified assumptions, the simulation results would not necessarily be consistent with every practical borehole. However, the simulation revealed general trends that can strengthen or improve our existing understanding and validate the previously proposed conceptual model.

5 Discussion

Sedapp is a diffusion-based model and its transport coefficient is a function of both distance from estuary and water depth. Compared with most existing diffusion models based only on water depth, this modification has great advantages in fluvial-deltaic environments, especially for 2DH scenarios. Sedapp not only simulates some surface landscapes, but it also reveals some interesting internal features. In the sections beside the channel in Model 1, the formation rate of the clinoforms had a close relationship with distance between the channel and the section. This may be of great significance for analyzing ancient strata. Considering the resolution of seismic data, it is easier to observe changes in the density of the foreset than to directly find a channel. This may provide some important supplementary information in areas with less borehole data.

Sedapp also showed strong simulation ability in 1DH scenarios. It was not only sufficient for the shallow marine environment, but also for the simulation of a continental fault basin (Fig.11). The simulation results were similar to previous studies (Li et al., 2018). In addition, Sedapp can avoid some potential problems that water depth models may not overcome. For example, when the slope is steep, the slope break trajectory created by the water depth model can even become far above the shoreline (Fig.12a and c). In contrast, Sedapp does not face such a problem. As long as the sea level is constant, the slope break line will remain in a straight line and the clinoforms will also move smoothly to the ocean (Fig.12b and d).

The transport coefficient is a relatively long-term geomorphologic physical quantity, while wave, tidal, and current energy are relatively short-term hydrodynamic quantities. However, they are closely related. A river entering the sea is a type of jet flow phenomenon. The flow velocity decreases rapidly from the river mouth to the sea, which also has a strong negative correlation with the distance to the mouth of the river. The contour map of water flow velocity is fan-shaped. At the same time, the decrease of velocity is also an important cause of sediment deposition, which also explains the close fan-shaped morphology of a delta front. Correspondingly, an increase in water depth will also decrease the flow velocity. For the open coast without river injection, a model based on water depth seems to be reasonable. However, for a coast with river injection, it is difficult to explain the formation of the fan-shaped morphology of a delta. Therefore, it can be concluded that, in more general cases, the transport coefficient should be a function of short-term water energy, which is related to both the

estuary distance and the water depth. When there is river injection, the river process is dominant and

300   the estuary distance function is a reasonable proxy for the transport coefficient. When there is no river

injection, the water depth plays the main role. In addition, particle size is also a decisive factor (Nash

1980; Andrews and Bucknam 1987). Hence, a choice function (see Eq. (9)) and differentiated α's are

used to adapt different environments and lithologies. Although the current results of Sedapp seem

plausible, these settings for transport coefficient are still empirical. Due to the complex nature of the

305   tranformation from short-term processes to long-term ones, it is difficult to build an accurate bridge

between sediment hydrodynamics and stratigraphic formation, which may be the focus of the next step.

6 Code availability

The current version of model is available from the project website:

http://zenodo.org/record/4556868 or https://github.com/lijingzheQD/Sedapp_v2021 under the Creative

310   Commons Attribution 4.0 International License. The exact version of the model used to produce the

results used in this paper is archived on Zenodo. Input data and scripts of the case studies are also

presented in this site. For more details about Sedapp, please contact Jingzhe Li via email

lijingzhe@qust.edu.cn .

Contribution of each author

315   JL developed the main algorithm of Sedapp and took the lead in writing the manuscript. PL

developed the FVM solver for Sedapp. PL, SS, ZS, YZ, LG, JZ and DD participated in the conceiving

of the presented idea. SS supervised the project.

Competing interests

No conflict of interest exits in this manuscript.

320   **Acknowledgement**

Financial support was provided by the National Natural Science Foundation of China (42002169),

the Initial Fund for Young Scholars of Qingdao University of Science and Technology, and the

Research Funding from King Abdullah University of Science and Technology (KAUST) through the

grants BAS/1/1351-01. Jingfa Li from Beijing Institute of Petrochemical Technology, Jie Chen from

325 Xi'an Jiaotong University and Hua Zhong from Guangdong University of Finance and Economics also

offered constructive advice. We would also like to thank John Armitage, an anonymous referee, and

the GMD editors for their constructive and helpful reviewing and editing work.

Reference

330   Andrews DJ, Bucknam RC. Fitting degradation of shoreline scarps by a nonlinear diffusion model. Journal of Geophysical Research: Solid Earth. 1987 Nov 10;92(B12):12857-67.

Armitage, J. J., Duller, R. A., Whittaker, A. C., & Allen, P. A. (2011). Transformation of tectonic and climatic signals from source to sedimentary archive. Nature Geoscience, 4(4), 231-235.

Armitage, J. J., Whittaker, A. C., Zakari, M., & Campforts, B. (2018). Numerical modelling of
335   landscape and sediment flux response to precipitation rate change. Earth Surface Dynamics, 6(1), 77-99.

Athy, Lawrence Ferdinand. "Density, porosity, and compaction of sedimentary rocks." Aapg Bulletin 14, no. 1 (1930): 1-24.

Dalman RA, Weltje GJ. SimClast: An aggregated forward stratigraphic model of continental
340   shelves. Computers & geosciences. 2012 Jan 1;38(1):115-26.

Ding X, Salles T, Flament N, et al. Quantitative stratigraphic analysis in a source-to-sink numerical framework. Geoscientific Model Development, 2019, 12(6).

Fernandes, Nelson F., and William E. Dietrich. "Hillslope evolution by diffusive processes: The timescale for equilibrium adjustments." Water Resources Research 33, no. 6 (1997): 1307-1318.

345   Granjeon, D. 3D forward modelling of the impact of sediment transport and base level cycles on continental margins and incised valleys. From Depositional Systems to Sedimentary Successions on the Norwegian Continental Margin (2014): 453-472.

Guerit, L., Yuan, X. P., Carretier, S., Bonnet, S., Rohais, S., Braun, J., & Rouby, D. (2019). Fluvial landscape evolution controlled by the sediment deposition coefficient: Estimation from experimental
350   and natural landscapes. Geology, 47(9), 853-856.

Kaufman P, Grotzinger JP, McCormick DS, Franseen EK, Watney WL. Depth-dependent diffusion algorithm for simulation of sedimentation in shallow marine depositional systems. InSedimentary Modeling: Computer Simulations and Methods for Improved Parameter Definition 1991 (Vol. 233, pp. 489-508). Kansas Geological Survey Bulletin.

355   Li J, Liu P, Zhang J, Sun S, Sun Z, Du D, Zhang M. Base Level Changes based on Basin Filling Modelling: a Case Study from the Paleocene Lishui Sag, East China Sea Basin.Petroleum Science, 2020, 17 (5). https://doi.org/10.1007/s12182-020-00478-2

Li J, Zhang J, Sun S, Zhang K, Du D, Sun Z, Wang Y, Liu L, Wang G. Sedimentology and mechanism of a lacustrine syn-rift fan delta system: A case study of the Paleogene Gaobei Slope Belt,
360   Bohai Bay Basin, China. Marine and Petroleum Geology. 2018 Dec 1;98:477-90.

Liu P, Yao J, Couples G D, et al. Numerical modelling and analysis of reactive flow and wormhole formation in fractured carbonate rocks. Chemical Engineering Science, 2017, 172: 143-157.

Miall, A. D. (2016). Stratigraphy: the modern synthesis. In Stratigraphy: A modern synthesis (pp. 382-386). Springer, Cham.

365   Moukalled F, Mangani L, Darwish M. The finite volume method in computational fluid dynamics. Berlin, Germany:: Springer; 2016.

Muto T, Steel RJ. Role of autoretreat and A/S changes in the understanding of deltaic shoreline trajectory: a semi‐quantitative approach. Basin Research. 2002 Sep 1;14(3):303-18.

Nash DB. Morphologic dating of degraded normal fault scarps. The Journal of Geology. 1980
370   May 1;88(3):353-60.

Paola C. Quantitative models of sedimentary basin filling. Sedimentology. 2000 Feb;47:121-78.

Pelletier, Jon. "Fundamental Principles and Techniques of Landscape Evolution Modeling." In

Treatise on Geomorphology, pp. 29-43. Elsevier Inc., 2013.

375 Rivenaes JC. Application of a dual‐lithology, depth‐dependent diffusion equation in stratigraphic simulation. Basin Research. 1992 Jun 1;4(2):133-46.

Rivenaes JC. Impact of sediment transport efficiency on large‐scale sequence architecture: results from stratigraphic computer simulation. Basin Research. 1997 Jun;9(2):91-105.

Sclater JG, Christie PA. Continental stretching: An explanation of the post‐mid‐Cretaceous subsidence of the central North Sea basin. Journal of Geophysical Research: Solid Earth. 1980 Jul
380 10;85(B7):3711-39.

Syvitski JP, Hutton EW. 2d sedflux 1.0 c:: an advanced process-response numerical model for the fill of marine sedimentary basins. Computers & Geosciences. 2001 Jul 1;27(6):731-53.

Versteeg HK, Malalasekera W. An introduction to computational fluid dynamics: the finite volume method. Pearson education; 2007.

385 Yuan XP, Braun J, Guerit L, Simon B, Bovy B, Rouby D, Robin C, Jiao R. Linking continental erosion to marine sediment transport and deposition: A new implicit and O (N) method for inverse analysis. Earth and Planetary Science Letters. 2019 Oct 15;524:115728.

Zhang J, Sylvester Z, Covault J. How do basin margins record long-term tectonic and climatic changes?[J]. Geology, 2020.

390
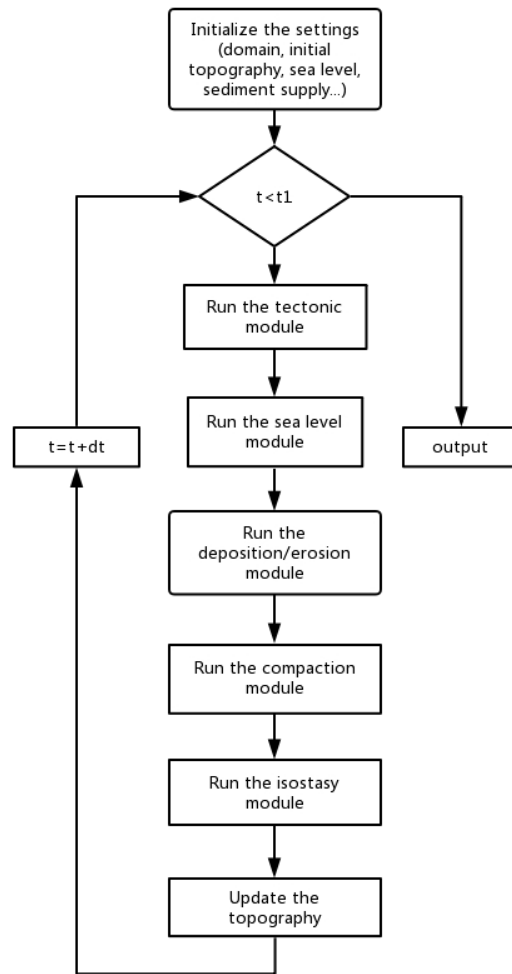
Fig. 1 Flowchart of the algorithms in Sedapp
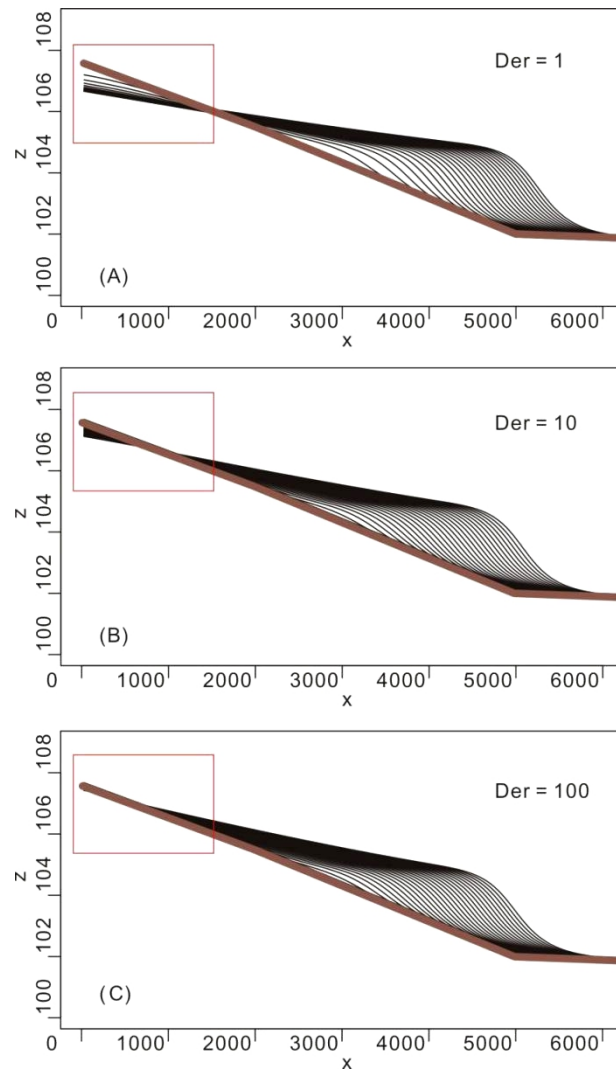
Fig. 2 Dip direction section with different Der values (Der = 1, Der = 10, Der = 100 respectively).

395   Erosion will be switched off if Der is large enough.
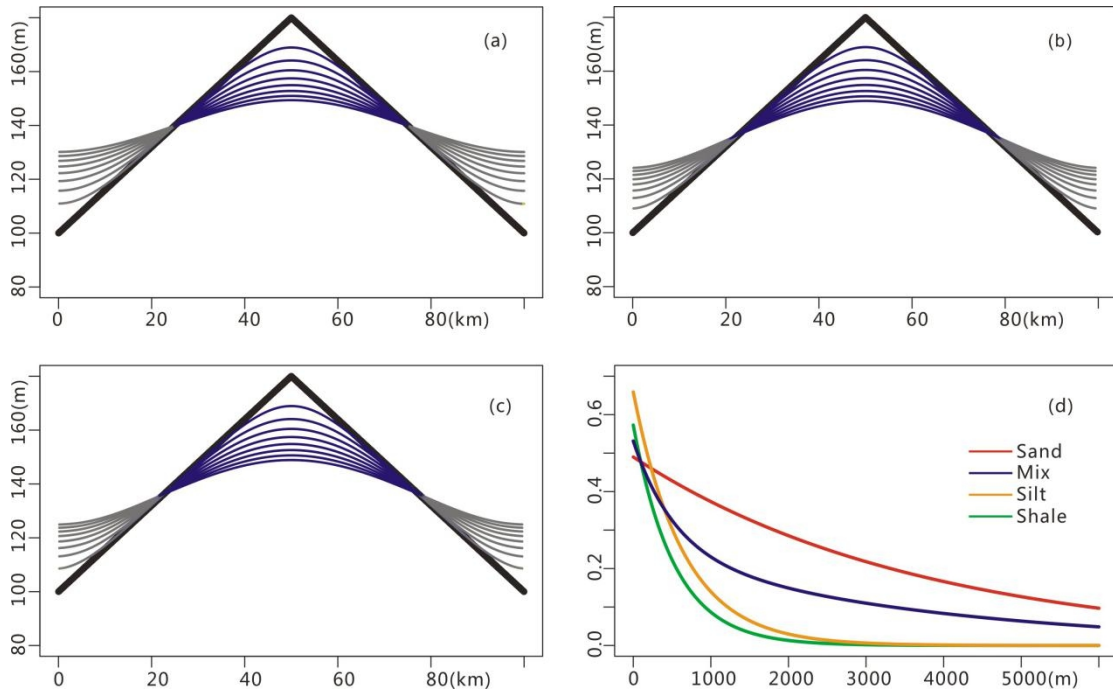
Fig. 3 Customized compaction and the porosity curves. a) the x-z plot with original

depth-porosity scale; b) the x-z plot with magnified depth-porosity scale (x100) to enhance compaction;

c) the x-z plot with magnified depth-porosity scale (x1000) to enhance compaction; d) Depth-porosity

400   curves used in the compaction module (the mix indicates mixed 50%-50% sand and shale. Details see

Athy, 1930; Sclater and Christie 1980)
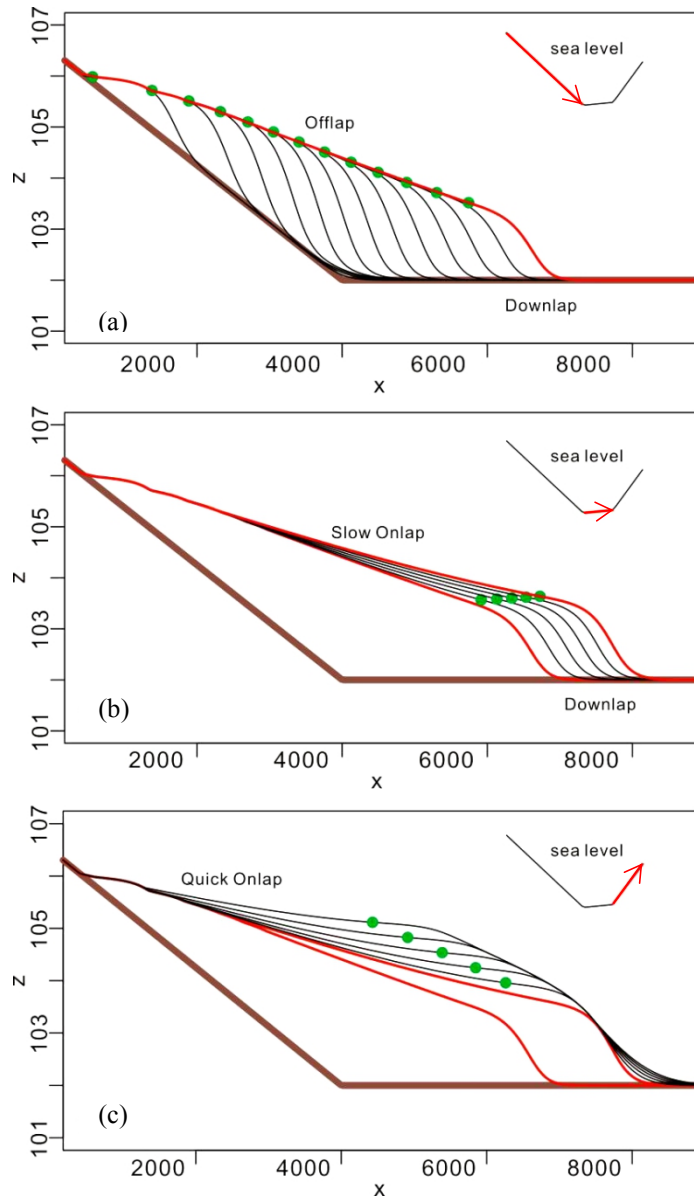
Fig. 4 Typical stacking patterns acquired through different sea level change rates
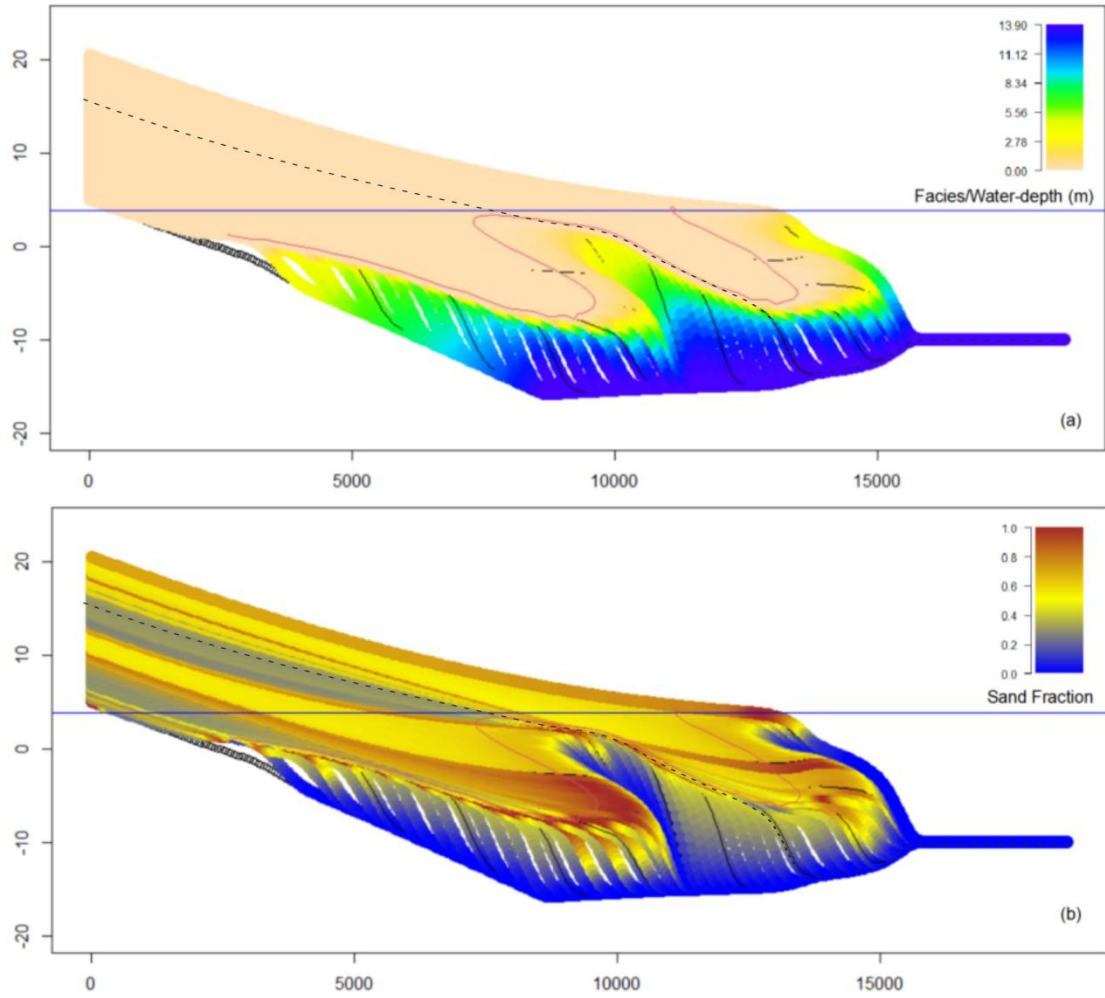
405   Fig. 5 Simulated stratigraphy under two full sea level cycles. A) facies section and B) lithological

section.
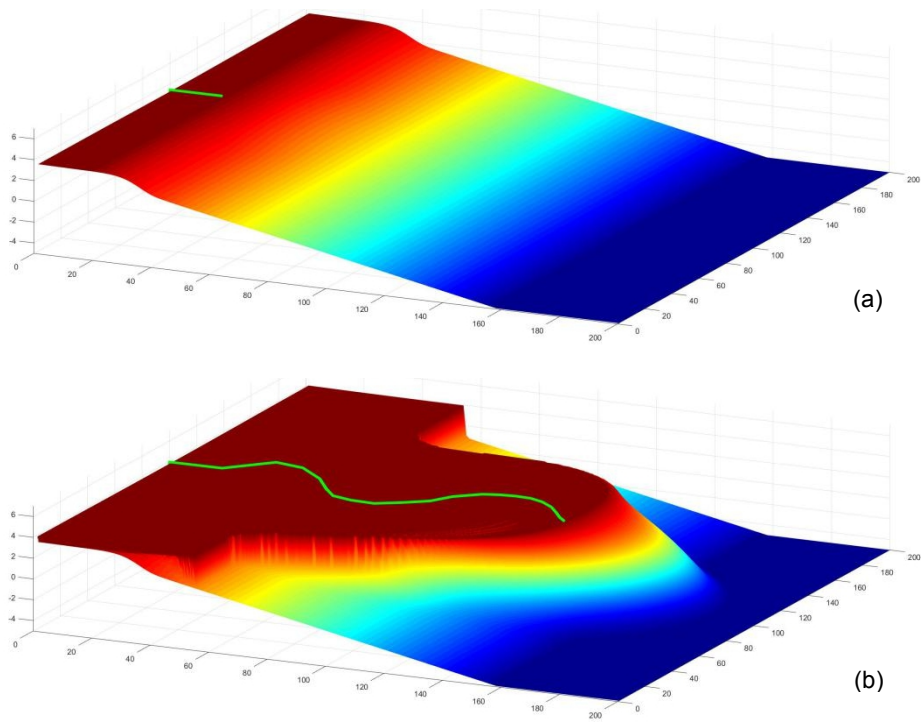
410   Fig. 6 The initial topography and the simulated results of Model 1. (a): the initial topography; (b):

the topography at t=10 Myr.
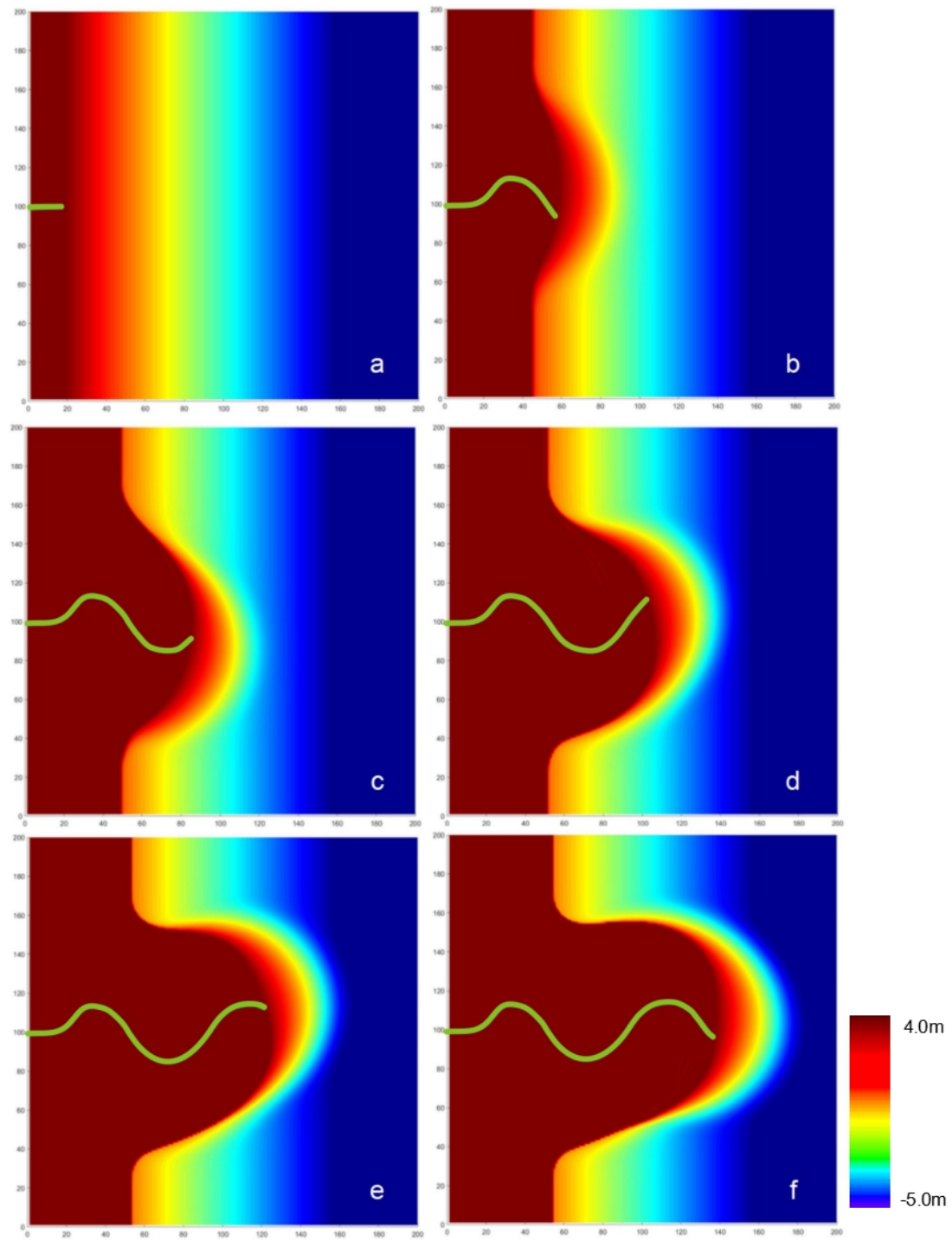
Fig. 7 Plane view of Model 1 results. (a): t=0Myr; (b): t=2 Myr; (c): t=4Myr; (d) t=6Myr; (e) t=8Myr; (f) t=10Myr.

415
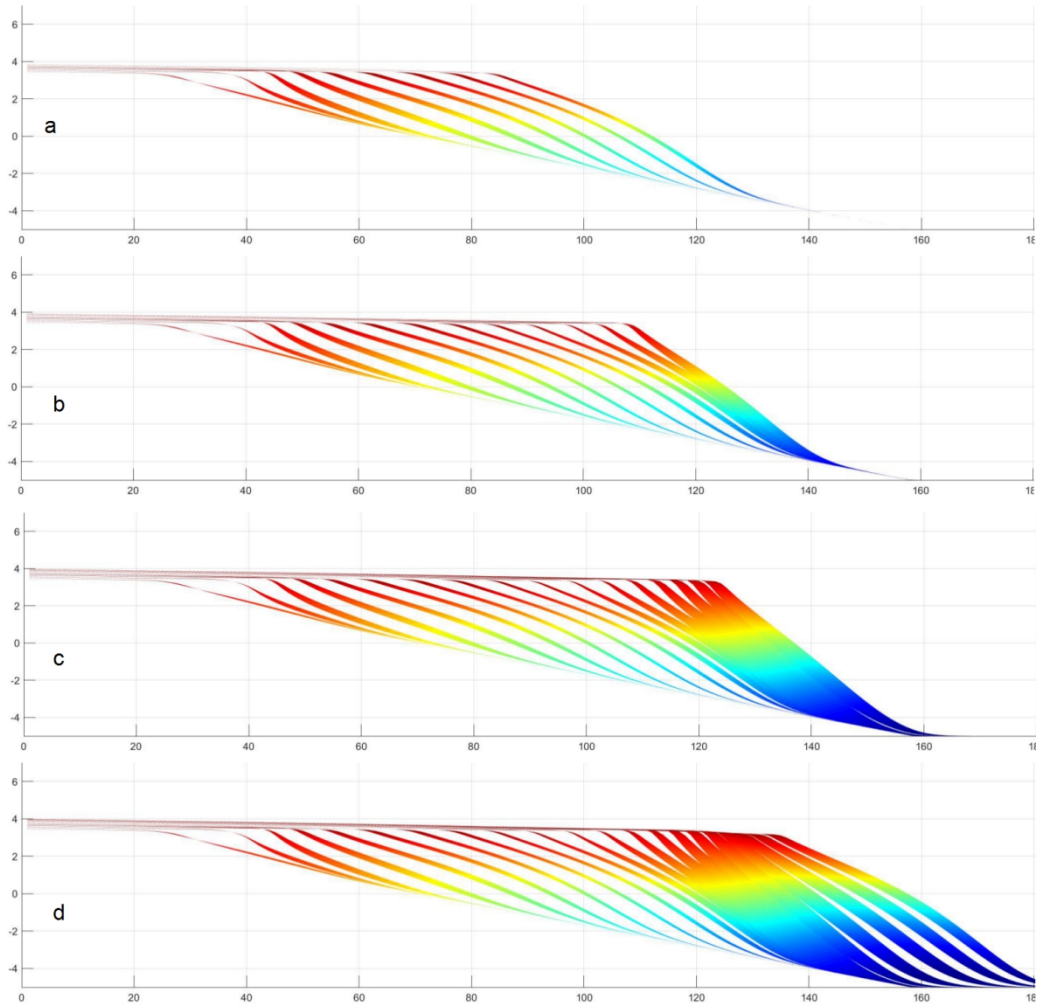
Fig. 8 Cross section at x=75m. (a): t=4Myr; (b): t=6 Myr; (c): t=8Myr; (d) t=10Myr.
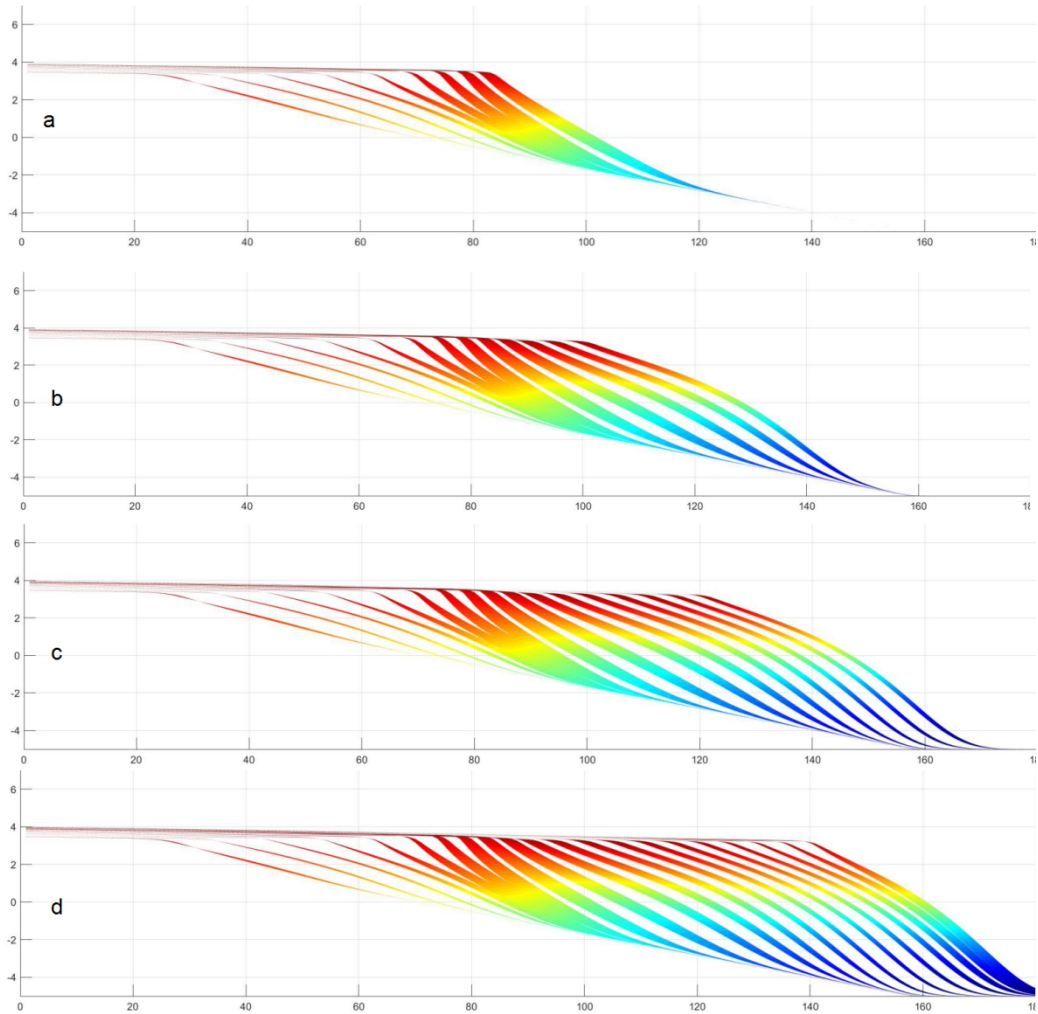
Fig. 9 Cross section at x=125m.   (a): t=4Myr; (b): t=6 Myr; (c): t=8Myr; (d) t=10Myr.

Fig. 10 Horton River Delta in Canada (a) and Ebro Delta in Mediterranean Sea (b) (taken from ©

Google Maps)

420
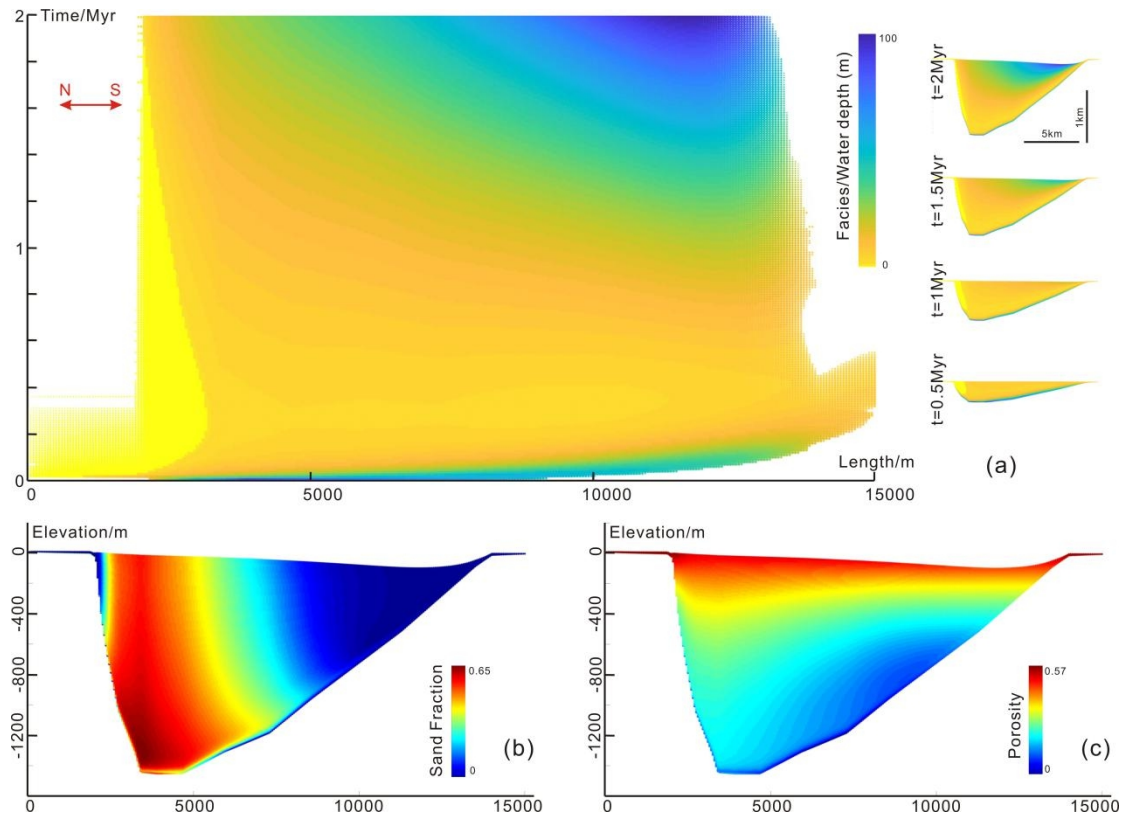
Fig. 11 Simulation results of Gaobei Slope Belt during the study interval. a) Sedapp results of facies in the time domain (Wheeler diagram) and depth domain at different times; b) Sedapp results of sand fraction in the depth domain. c) Sedapp results of porosity in the depth domain
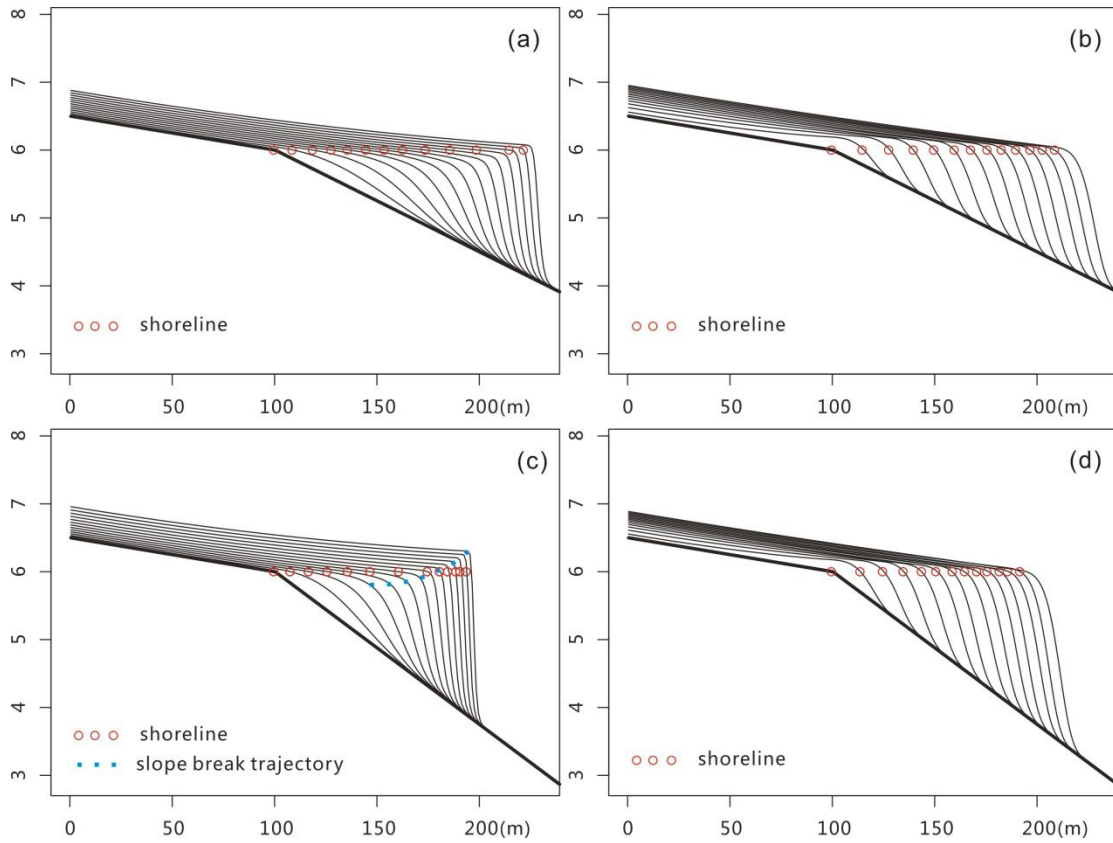
Fig. 12 Comparison of the simulated results by water-depth based algorithm and the algorithm of

430 Sedapp. a) Clinoforms of gentle slope created in water depth models; b) Clinoforms of gentle slope

created in Sedapp; a) Clinoforms of steep slope created in water depth models; d) Clinoforms of steep

slope created in Sedapp. The results of the two algorithms did not diverge strongly when the original

slope was gentle, while the clinoform shapes and slope break trajectories could be very different when

the slope was steep.

435 Tab. 1 Main simulation parameters of Model1 (see 2.1 above for meanings of the notations)

Parameter	Value
α	1000
β	500
η	2
α_{wd}	10000
β_{wd}	0.16
η_{wd}	1
ε	0
Der	1